Molecular dynamics simulations of the mechanisms controlling the propagation of bcc/fcc semi-coherent interfaces in iron

Ou, Xiaoqin; Sietsma, Jilt; Santofimia Navarro, Maria

DOI
10.1088/0965-0393/24/5/055019

Publication date
2016

Published in
Modelling and Simulation in Materials Science and Engineering

Molecular dynamics simulations of the mechanisms controlling the propagation of bcc/fcc semi-coherent interfaces in iron

2016 Modelling Simul. Mater. Sci. Eng. 24 055019

(http://iopscience.iop.org/0965-0393/24/5/055019)

OPEN ACCESS
IOP Publishing
Modelling and Simulation in Materials Science and Engineering
Modelling Simul. Mater. Sci. Eng. **24** (2016) 055019 (18pp) doi:10.1088/0965-0393/24/5/055019

Molecular dynamics simulations of the mechanisms controlling the propagation of bcc/fcc semi-coherent interfaces in iron

X Ou, J Sietsma and M J Santofimia

Department of Materials Science and Engineering, Delft University of Technology, Mekelweg 2, 2628 CD Delft, The Netherlands

E-mail: X.Ou@tudelft.nl

Received 31 August 2015, revised 8 May 2016
Accepted for publication 20 May 2016
Published 14 June 2016

Abstract

Molecular dynamics simulations have been used to study the effects of different orientation relationships between fcc and bcc phases on the bcc/fcc interfacial propagation in pure iron systems at 300 K. Three semi-coherent bcc/fcc interfaces have been investigated. In all the cases, results show that growth of the bcc phase starts in the areas of low potential energy and progresses into the areas of high potential energy at the original bcc/fcc interfaces. The phase transformation in areas of low potential energy is of a martensitic nature while that in the high potential energy areas involves occasional diffusional jumps of atoms.

Keywords: molecular dynamics simulations, iron, interface, growth, martensitic transformation

(Some figures may appear in colour only in the online journal)

1. Introduction

Martensite forms from austenite during the quenching process of steels, which has been the subject of intensive studies [1, 2]. The formation of martensite involves a collective movement of atoms of less than an interatomic distance at a velocity possibly as high as that of sound [3]. Due to the difficulty in observing these atomic processes, experimental studies on the nature of martensitic transformation are limited. In recent years, molecular dynamics (MD) simulations have been shown to be a possible way to study phase transformation mechanisms in steels, including the martensitic transformation [4–6].

In steels, the structure, energy and kinetics of phase boundaries between ferrite (α-bcc) and austenite (γ-fcc) phases play a key role in phase transformations and microstructure formation [7]. During the martensitic transformation, the coordinated movement of atoms leads to a specific orientation relationship between the parent austenite (γ) and newly formed ferrite (α) lattices, in which a pair of close-packed planes in the α and γ phases are parallel or nearly parallel. Besides, the corresponding closest-packed directions within these planes are roughly parallel too. Bain [8] proposed a possible fcc-to-bcc transformation path by identifying a bct unit cell in the fcc crystal. The mechanism proposed by Bain involves a contraction of the z-axis by about 21% and an expansion of the x, y-axes by about 12%. However, the orientation relationship between the fcc parent phase and bcc martensite through the simple Bain contraction and elongation of axes is different from the ones mainly observed in experiment [9]. Other fcc-to-bcc transformation paths result in the Nishiyama–Wassermann (NW) [10] or Kurdjumov–Sachs (KS) [11] orientation relationships (ORs). They imply similar mechanisms of transformation with the Bain transformation but introduce a main shear in the $\langle 1\,1\,2\,\rangle$ direction of the $\{1\,1\,1\}$ plane. In previous studies, the effects of semi-coherent bcc/fcc interfaces with the NW or KS OR on the fcc-to-bcc transformation in pure iron have been investigated by MD simulations [12–19]. However, the mechanisms that were found to control the fcc-to-bcc transformation vary significantly for different simulations, considering the differences of bcc/fcc interface orientations and the embedded atom method (EAM) potential used.

One of the main contradictions arises from the growth mechanisms of the original bcc phase in these systems [4, 12–19]. Bos *et al* [4] studied two interfaces close to the Bain OR and KS OR using the Johnson and Oh potential [20]. The interface motion involved the majority of atoms moving collectively over less than one interatomic distance during the transformation, which indicated a martensitic mechanism for the growth of the original bcc phase. Besides, dislocation glide occurred along closely packed planes in both the fcc and bcc crystalline structures during the martensitic transformation. Wang and Urbassek [14, 18] studied a bcc/fcc interface with the NW OR using the Meyer–Entel [21] potential. A martensitic mechanism was determined for the fcc-to-bcc transformation at the fcc/bcc interfaces, which slightly roughened during proceeding into the original fcc phase. The bcc/fcc interface studied by Song and Hoyt [16, 17] was tilted by 4.04° about the NW OR using the Ackland potential [22], thus a series of parallel steps (or primary structural disconnections) was introduced into the interfaces. The mobile interface did not migrate by a martensitic mechanism but by the rapid advance of the mobile defects forming on the primary disconnections.

Considering these contradictions from literature, three systems with different semi-coherent bcc/fcc interfaces are introduced in the present paper to investigate the mechanisms controlling the growth of the original bcc phase in iron by MD simulations. Mechanisms controlling the growth of the original bcc phase at the bcc/fcc interfaces for the three systems are studied in detail based on the atomic configuration during the transformation and the energy distribution of the atoms.

2. Simulation conditions

The Mendelev potential [23] used in the present work describes the bcc phase to be stable in the temperature range of 0 to 1820 K. It has been successfully employed in describing the martensitic transformation in iron with bcc/fcc interfaces by MD simulations [24, 25], for which two systems with bcc/fcc interfaces in the Pitsch OR and KS OR were studied. The deformation induced γ (fcc) $\rightarrow$ ε(hcp) $\rightarrow$ α'(bcc) martensitic transformation was observed at the diffusing bcc/fcc interfaces in the MD simulations based on the Mendelev potential [23], which

Table 1. Systems studied in this work. x, y, and z denote the lengths of the systems in the three Cartesian directions.

System	x (Å)	y (Å)	z (Å)	x_{bcc} UC	y_{bcc} UC	z_{bcc} UC	x_{fcc} UC	y_{fcc} UC	z_{fcc} UC	fcc atoms	bcc atoms
NW, $(1\,1\,1)_{fcc} \parallel (1\,1\,0)_{bcc}$, $[\bar{1}\,1\,0]_{bcc} \parallel [\bar{1}\,\bar{1}\,2]_{fcc}$,											
	205.91	82.76	91.06	51	29	10	23	16	8	706 56	591 60
KS, $(1\,1\,1)_{fcc} \parallel (1\,1\,0)_{bcc}$, $[\bar{1}\,1\,2]_{bcc} \parallel [\bar{1}\,\bar{1}\,2]_{fcc}$,											
	223.79	113.74	91. 06	32	23	10	25	22	8	105 600	883 20
Nagano, $(1\,1\,\bar{2})_{fcc} \parallel (1\,1\,0)_{bcc}$, $[\bar{1}\,1\,0]_{bcc} \parallel [1\,1\,1]_{fcc}$,											
	278.59	82.77	112.06	69	29	10	44	16	8	135 168	800 40

Note: Lengths are indicated both in Å and unit cells (UC).

coincides with experimental observations using the high resolution transmission electron microscopy (HRTEM). Besides, the potential is in better agreement with the experimental lattice parameter, elastic constants, point-defect energies, bcc–fcc transformation energy, liquid density, liquid structure factor, melting temperature and other properties than other existing EAM iron potentials [23]. It provides a better coincidence of the cohesive energy difference (or the driving force) $\Delta E_{fcc-bcc}$ between the bcc and fcc phase with the density functional theory (DFT) results as well [26].

The two well-known crystallographic orientation relationships between the austenite and ferrite phases in steel are the NW and the KS ORs [27], which are described as:

$$\text{N– W: } (1\,1\,0)_{bcc} \parallel (1\,1\,1)_{fcc},\ [0\,0\,1]_{bcc} \parallel [1\ \bar{1}\,0]_{fcc}$$

$$\text{K– S: } (1\,1\,0)_{bcc} \parallel (1\ 1\ 1)_{fcc},\ [1\ \bar{1}\,1]_{bcc} \parallel [1\ \bar{1}\,0]_{fcc}$$

Both relationships have the closest packed planes in the two phases parallel: $\{1\,1\,1\}_{fcc} \parallel \{1\,1\,0\}_{bcc}$. In this work, the studied systems with the above two interfaces are called System NW and System KS, respectively. Besides, a third semi-coherent bcc/fcc interface with higher interfacial energy is also studied. In this work, the orientation of this third interface will be identified with the name 'Nagano OR' and the corresponding system as 'System Nagano'. The interface with the Nagano OR originates from the previous studies by Nagano and Enomoto [7], in which a high energy interface was obtained by rotating the fcc bulk of the NW system over 90° around the $[0\,0\,1]_{\alpha} \parallel [\bar{1}0\,1]_{\gamma}$ axis.

The detailed information of the three systems is listed in table 1. The simulation was performed assuming periodic boundaries in all three directions and in absence of free surfaces. The dimensions in the x and y directions were carefully chosen to ensure that the elastic strain due to volume mismatch is kept to a minimum. The mismatches in x and y directions are 0.08% and 0.03% for System NW, 0.10% and 0.07% for System KS, 0.07% and 0.03% for System Nagano, respectively. These small strains imply stresses less than 150 MPa, leading to negligible additional strain energy. Lattice parameters for fcc (3.658 Å) and bcc (2.855 Å) are obtained at 0 K and the potential-energy difference between the fcc and bcc phase at 0 K is 0.122 eV per atom. From experimental studies lattice parameters at 0 K are concluded for fcc and bcc to be 3.562 Å and 2.860 Å, respectively [22].

The method of energy minimization was used to relax the system. Relaxation was performed as follows: all atoms in fcc bulk were fixed while the atoms in the bcc bulk phase were allowed to move in the z direction. Thus the simulation box can expand/contract perpendicular

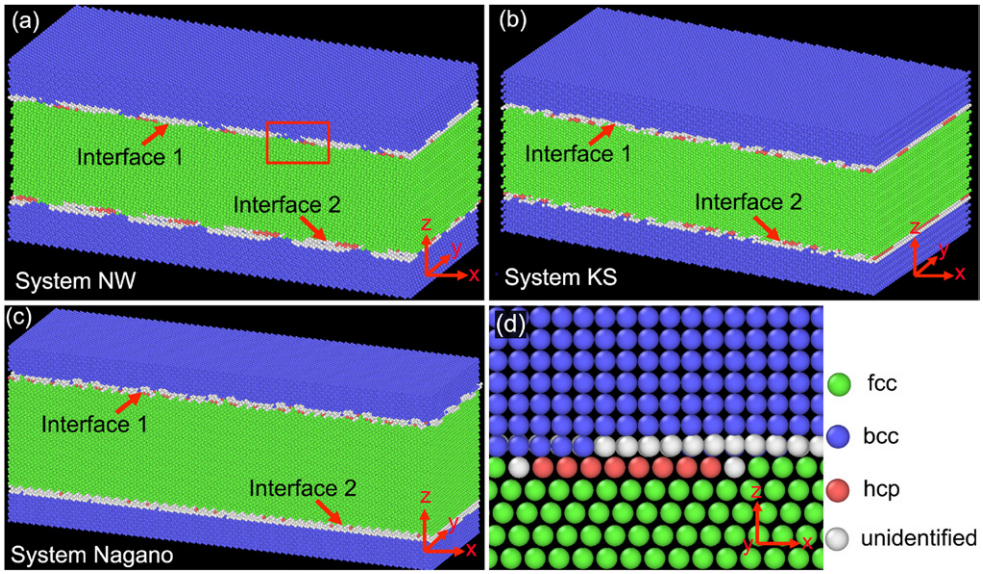

Figure 1. The initial, relaxed configurations of (a) System NW, (b) System KS and (c) System Nagano. (d) Represents the enlarged region as inside the red rectangular in figure (a). Colours represent different phase structures: blue-bcc; green-fcc; red-hcp; white-unidentified.

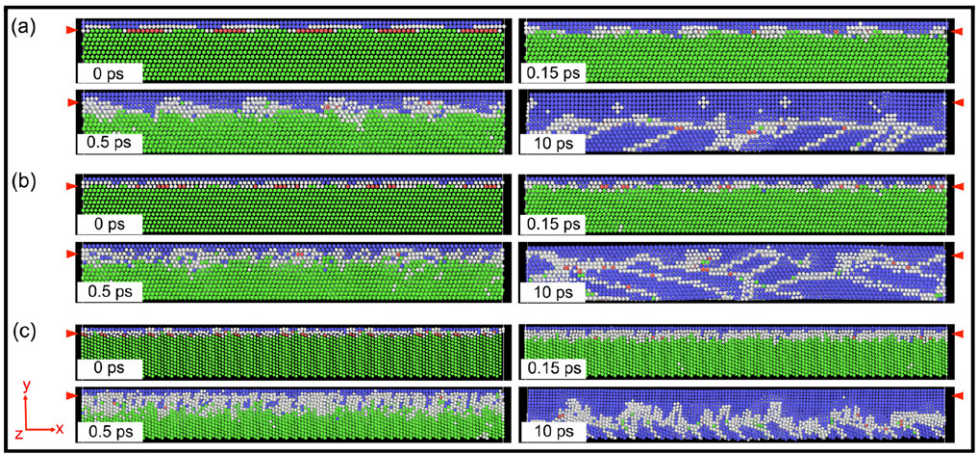

Figure 2. Propagation of one of the bcc/fcc interfaces of (a) System NW, (b) System KS and (c) System Nagano, respectively. The position of the original bcc/fcc interface is marked by a red triangle in each configuration. Colours represent different phase structures: blue-bcc; green-fcc; red-hcp; white-unidentified.

to the phase boundary, so that the high stress caused by the phase misfit at the phase boundary is reduced. The dimensions of the box in the x and y directions were not changed during relaxation. The pressure perpendicular to the interface relaxed to less than 20 MPa.

After energy minimization, the relaxed configuration was used as the initial configuration in the following simulations. The simulations were performed at constant pressure and temperature, using a barostat and a thermostat of the Nosé–Hoover type at 300 K under the

pressure of 10^5 Pa (NPT ensemble). The MD time step was fixed at 0.000 50 ps per step and the simulations for System NW, KS and Nagano last for a total time of 1000, 1000 and 1500 ps, respectively. Calculations were performed with the open-source LAMMPS code [28].

To reveal the atomistic mechanisms related to the fcc-to-bcc transformation, a discriminator needs to be used to determine atoms as belonging to either the fcc or bcc phase. Stukowski [29] proposed a simple extension to the common neighbour analysis (CNA) method as the adaptive common neighbour analysis (a-CNA) method that made it suitable for multi-phase systems. Therefore the a-CNA was chosen as the discriminator in the present study. The configurations are displayed using the software OVITO [30].

The snapshot shown in figure 1 represents the initial, relaxed configurations for the three systems. The lattice mismatch of fcc/bcc atoms at the boundaries resulted in the hcp or unidentified structures of some atoms. The system always contained two bcc/fcc interfaces perpendicular to the z direction considering the periodicity conditions. Each bcc/fcc interface includes two monolayers: one fcc layer and the other bcc layer, as shown by figure 1(d), which shows the enlarged region inside the red rectangular in figure 1(a).

3. Results and discussion

3.1. Growth of the bcc phase at the bcc/fcc interfaces

Figure 2 shows the propagation of the bcc/fcc interfaces at 0, 0.15 0.5 and 10 ps in System NW (a), System KS (b) and System Nagano (c), respectively. In each configuration, only 2 bcc planes plus 12 fcc planes perpendicular to the bcc/fcc interface are included. It is found that the original bcc phase starts propagating into the fcc phase at 0.05 ps. The facetted growth of the original bcc phase is then observed for the three systems, as shown by the configurations at 0.15 and 0.5 ps in figures 2(a)–(c). The bcc/fcc interface propagation involves up to 7 atomic layers into the original fcc phase in the three systems between 0 ps and 1.0 ps. Nucleation of bcc phase takes place nearby the bcc/fcc interfaces and inside the fcc bulk at around 1.0 ps, which pins the further propagation of the interfaces.

The nucleation of bcc phase inside the fcc bulk was also observed in the MD simulations based on the Meyer–Entel Potential [21] by Wang and Urbassek [14, 18], in which the fcc-to-bcc transformation in iron with bcc/fcc interfaces in an NW or KS OR was studied. They observed homogeneous nucleation of bcc phase inside the fcc bulk in both systems, the growth of these bcc nuclei hindered the propagation of the original bcc/fcc interfaces. Similar to the results in the present studies, the bcc/fcc interfaces in the NW OR based on the Meyer–Entel potential [21] propagated into the original fcc bulk for some distance perpendicular to the interface plane, while the interfaces in the KS OR did not move into the fcc bulk significantly. However, only propagation of the bcc/fcc interface, but not the bcc nucleation inside the fcc bulk, was observed by Song and Hoyt [16, 17]. They studied the fcc-to-bcc transformation in iron with bcc/fcc interfaces rotated by 4.04° from the NW OR by MD simulations using the Ackland potential [22], and found that the bcc/fcc interfaces propagated into the original fcc bulk until the whole system transformed to a single bcc grain.

Considering that the bcc/fcc interface by Song and Hoyt [16, 17] was several degrees away from the perfect NW OR, the introduced defects at the interfaces might contribute to the propagation of the bcc/fcc interfaces into the whole fcc bulk. Figure 3 shows an examination performed by the present authors in iron with bcc/fcc interfaces in the regular NW OR, based on the Ackland Potential [22]. The results are compared with those based on the Mendelev potential [23]. As expected, the facetted propagation of the bcc/fcc interface in the NW OR is also observed in iron in the initial 0.5 ps with the Ackland potential [22]. The only difference

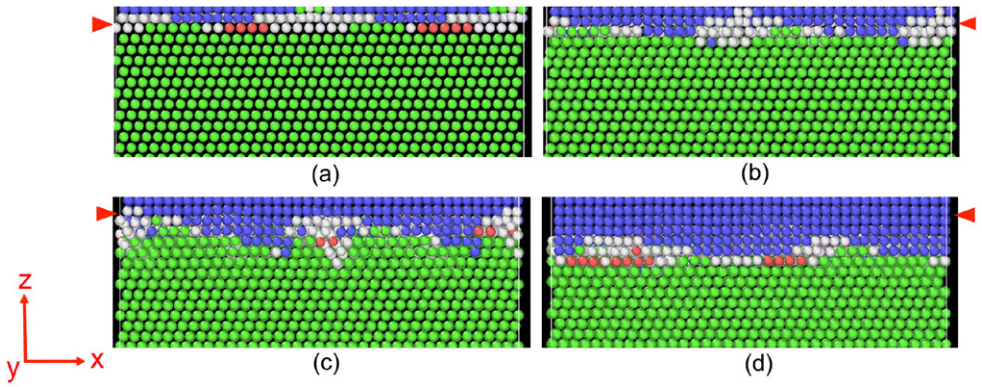

Figure 3. Propagation of one of the bcc/fcc interfaces in the NW OR in iron using the Ackland potential [22] at different simulation times: (a) 0 ps; (b) 0.15 ps; (c) 0.5 ps and (d) 10 ps. The position of the original bcc/fcc interface is marked by a red triangle in each configuration. Colours represent different phase structures: blue-bcc; green-fcc; red-hcp; white-unidentified.

is that earlier nucleation of bcc phase occurs in the fcc bulk with the Mendelev potential [23], as was reported by Wang and Urbassek [14, 18], due to its small energy barrier (less than 1 meV/atom) for a transition from fcc to bcc along the Bain path [26]. Nevertheless, the present study focuses on the transformation mechanisms at the bcc/fcc interfaces, excluding any effect resulting from the nucleation of bcc phase inside the fcc bulk. Similar observations related to the propagation of the bcc/fcc interfaces by the Mendelev potential [23] and the Ackland potential [22] indicate the same mechanism of the fcc-to-bcc transformation at the interfaces from both potentials. Besides, this study focuses on the results during the initial 0.5 ps, when the nucleation of bcc phase has not taken place yet. Thus the propagation of bcc/fcc interfaces in present paper is not affected by the bcc nucleation inside the fcc bulk. It should be noted that the facetted growth in System KS/Nagano is less obvious than that in System NW. Some parts of the interface in System KS do not move at all, as shown in the configuration at 10 ps of figure 2(b).

The present paper will focus on the fcc-to-bcc transformation through the bcc/fcc interface propagation during the first 0.5 ps. This phenomenon is studied focusing on the energy distribution of the atoms and the atomic configurations between the fcc and bcc planes at the interfaces. The original bcc/fcc interfaces in System NW, System KS and System Nagano include two layers: one mono bcc layer and the other fcc layer. The analysis focuses on the phase transformation on the fcc layer. The bcc layer at the interface is presented for a better view of the stacking of atoms between the original bcc and fcc planes. The potential energies of the bcc/fcc interfaces are studied. In present studies, for clarity in the comparisons between different configurations, the low-energy areas and high-energy areas are considered as the areas with potential energies corresponding to the lowest 20% and highest 60% of the corresponding colour bars in each individual configuration for System NW, System KS and System Nagano, respectively.

3.1.1. System NW. Figure 4(a) the superposed view of the $(1\,1\,1)_{fcc}$ and $(1\,1\,0)_{bcc}$ planes at the matching area of the interface with NW OR at 0 ps. The atoms are coloured according to their potential energy, which is found in the range of −3.960 eV to −3.470 eV. Wang and Urbassek [18] also studied the potential energy of atoms on the interface plane with the NW OR and found that

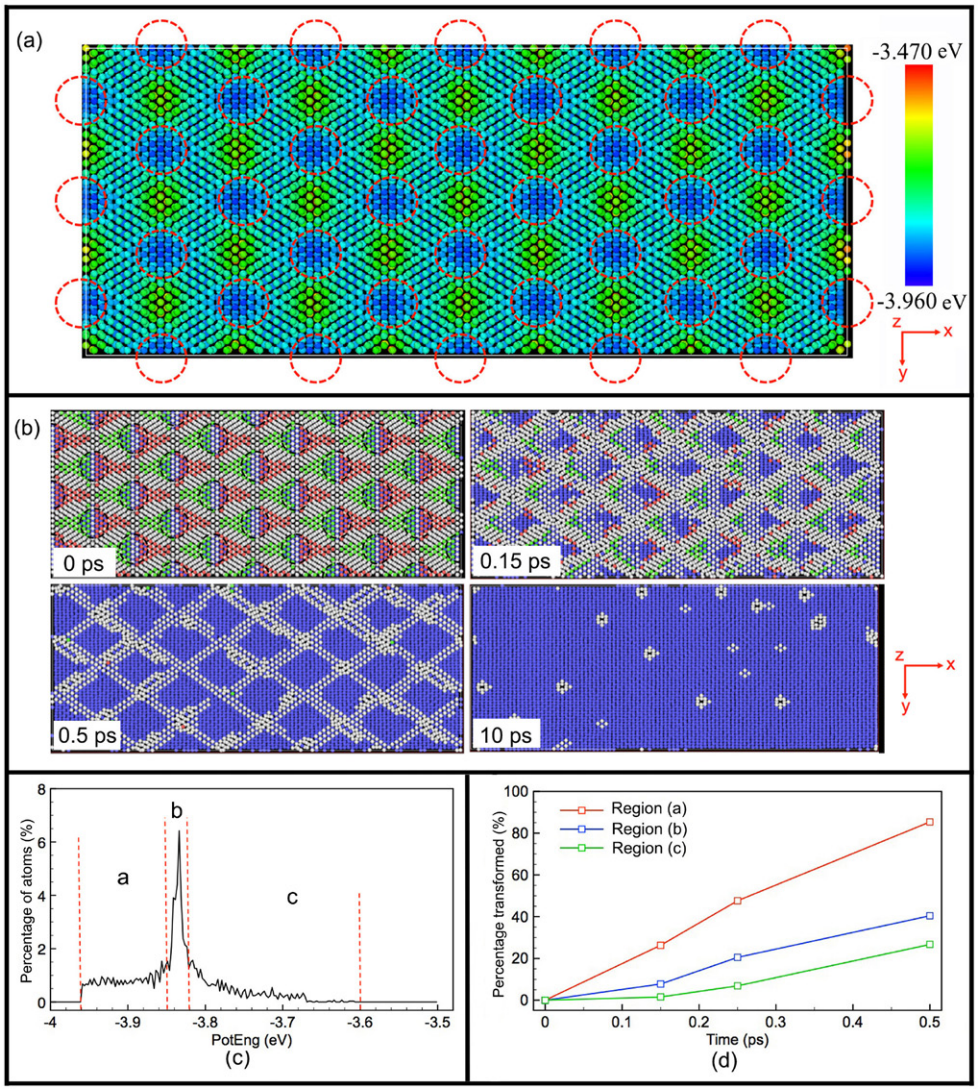

Figure 4. (a) Superposed view of $(1\,1\,1)_{fcc}$ and $(1\,1\,0)_{bcc}$ planes at the matching area of the interface with NW OR at 0 ps. Atoms have been coloured according to their potential energy, as the colour bar shows; (b) Phase transformation in the original fcc/bcc interfacial planes consisting of one fcc layer and one bcc layer in System NW. The colours denote the local crystal structures as in figure 1; (c) Energy distribution of atoms in the fcc monolayer at the original fcc/bcc interface in System NW at 0 ps; (d) Time evolution of the fraction of atoms transformed to bcc in individual regions in the fcc monolayer at the original fcc /bcc interface in the NW OR.

the original periodic structure of the interface was strongly disturbed after the relaxation process. In the present study, however, the bcc/fcc interfaces is less affected as the low-energy areas, in red dashed circles, appear periodically to some degree. The low-energy areas are located where atoms on the fcc mono layer have potential energies in the range between −3.960 eV and −3.862 eV, as 20% of the range of the colour bar in figure 4(a). It is calculated that 30.5% of atoms on the fcc layer belongs to the low-energy areas. Correspondingly, the high-energy areas

Table 2. Number of atoms in the monolayer of fcc plane at the original fcc/bcc interface at 0 ps.

System	N_{total}	N_a/N_{total}	N_b/N_{total}	N_c/N_{total}
NW		(−3.96, −3.85) eV	(−3.85, −3.82) eV	(−3.82, −3.60) eV
	2944	1064	1034	846
KS		(−4.0, −3.85) eV	(−3.85, −3.80) eV	(−3.80, −3.5) eV
	4400	1410	1921	1069
Nagano		(−4.0, −3.65) eV	(−3.65, −3.0) eV	—
	4224	2816	1408	—

Note: N_{total} represents the total number of atoms in the monolayer of fcc plane; N_a, N_b and N_c are the number of atoms distributed in potential energy ranges (a)–(c).

are those with potential energies ranged between −3.764 eV and −3.470 eV, which takes 60% of the height of the whole colour bar in figure 4(a). 10.6% of atoms belonging to the high-energy areas and the remaining areas have the intermediate potential energies.

Figure 4(b) shows the time evolution of the phase transformation at the fcc/bcc interface with NW OR during 10 ps and the colours indicate the local atomic structure as those in figure 1. The areas in the black circles in figure 4(b) correspond to those in the red circles in figure 4(a), that is, low potential energy areas. It was found that some atoms in the fcc-plane at the bcc/fcc interfaces are unidentified or identified with an hcp structure. This is because atoms with an fcc and bcc structure have, of course, different atomic surroundings. At the bcc/fcc interfaces, atoms can have a mixture of fcc- and bcc-surroundings and therefore are either unidentified or recognized with an hcp structure. Similarly, atoms near grain boundaries or vacancies may also be unidentified. From snapshots at 0.15 and 0.5 ps in figure 4(b), it is found that the fcc-to-bcc transformation involving the growth of the original bcc phase starts from the low-energy areas and finalizes at the high-energy areas at the interface. This finding will be analysed in detail in the next paragraph. Defects, i.e. vacancies, are found to remain at the sites where the final phase transformation takes place, as shown in the configuration at 10 ps in figure 4(b). This may be caused by density differences between the fcc and bcc crystals. It was reported by Tateyama *et al* [13] that atoms in the fcc region were rearranged into the bcc structure at the bcc/fcc interface to compensate for lattice mismatch during the sequential fcc-to-bcc transformation. The residual lattice mismatch may remain in the bcc structure since time for thermal relaxation was insufficient in the simulation time.

Table 2 shows the total number of atoms in the mono fcc-layer at the interface with NW OR as well as the number of atoms in the same mono fcc-layer having initial potential energies falling within three different ranges. The distribution of their initial potential energy is illustrated in figure 4(c). The number of fcc-atoms transforming to bcc is clearly related to their initial potential energy. This is explicitly shown in figure 4(d), where it is found that atoms tend to transform linearly with time in the three regions. It is estimated that the slopes are 190%, 82% and 27% for Regions (a)–(c), respectively. The slopes are calculated from data between 0 ps and 0.25 ps, which correspond to times well before a decrease of the transformation rate is observed. Transformation in Region (a), is faster than that in Region (b), which is followed by that in Region (c). The results indicate statistically that the growth of original bcc phase develops from low-energy areas to high-energy areas at the original bcc/fcc interfaces with NW OR.

3.1.2. System KS. Figure 5(a) is the superposed view of the $(1\,1\,1)_{fcc}$ and $(1\,1\,0)_{bcc}$ planes at the matching areas of the interface with KS OR at 0 ps. The potential energy is distributed

between −4.016 eV and −3.464 eV. The low-energy areas are marked in red dashed ellipses corresponding to areas in the black dashed ellipses in figure 5(b), which shows the development of the local crystallographic structure. The low-energy areas include atoms on the fcc mono layer with potential energies in the range between −4.016 eV and −3.906 eV. 13.9% of atoms on the fcc layer belongs to the low-energy areas. The high-energy areas are located where atoms have potential energies ranged between −3.795 eV and −3.464 eV. 22.7% atoms belonging to the high-energy areas. Similar to System NW, the growth of bcc phase at the original fcc/bcc interfaces in System KS starts from the low-energy areas, as seen from snapshots at 0.15 and 0.5 ps in figure 5(b). Then it develops into areas with high potential energies where eventually a number of defects, i.e. vacancies, are observed, as shown by the unidentified atoms at 10 ps.

Figure 5(c) shows the distribution of the potential energy of atoms in the mono fcc plane at the original bcc/fcc interfaces with KS OR. The potential energy is divided into Regions (a)–(c). The number of atoms distributed in the three regions at the initial configuration is included in table 2. Similar to System NW, atoms transforming to bcc during the initial 0.5 ps are mostly located in low-energy areas corresponding to Regions (a) and (b). The fraction of atoms transformed also follows a nearly linear relationship with time for each energy region (see figure 5(d)). It is estimated that the slopes are 138%, 53% and 10% for Regions (a)–(c), respectively. The slopes are also calculated before 0.25 ps as the same for System NW. However, the transformation at the interface with KS OR is slower than that with NW OR, as indicated by the lower gradient for each region in figure 5(d).

3.1.3. System Nagano. Figure 6(a) is the superposed view of $(1\,1\,\bar{2})_{\mathrm{fcc}}$ and $(1\,1\,0)_{\mathrm{bcc}}$ planes at the matching areas of the interface in Nagano OR at 0 ps. The atoms are coloured according to their potential energy, which ranges from −4.118 eV to −3.009 eV. The areas with low potential energy ranged between −4.118 eV and −3.896 eV is included in the red dashed ellipses. 11.8% of atoms on the mono fcc layer are included in the low-energy areas. Areas with potential energies between −3.674 and −3.009 eV are defined as high-energy areas. 33.3% atoms are included in these areas. The bcc phase grows from the low-energy areas to the high-energy areas in System Nagano, which can be seen from the snapshots at 0.15–10 ps in figure 6(b), similarly to System NW and System KS. Besides, vacancies are found at the end of the phase transformation, as labeled by the red arrow in figure 6(b).

The atoms in the mono fcc-plane at the interface are grouped into low-energy Region (a) and high-energy Region (b). The number of atoms falling in these two regions is included in table 2. Figure 6(c) shows the distribution of atoms in Regions (a) and (b) at 0 ps. It should be noted that, compared to System NW and System KS, a group of atoms on the fcc plane at the bcc/fcc interfaces have rather high potential energies, above −3.7 eV, and no atoms on the fcc plane at the original bcc/fcc interface have a potential energy in the range of −3.7 eV and −3.6 eV. This originates from the construction process of System Nagano, when an array of terraces is created by rotating the fcc bulk for 90° from the NW system around the $[0\,0\,1]_{\alpha} \parallel [\bar{1}\,0\,1]_{\gamma}$ axis. Defects at the terraces lead to the involved atoms having high potential energies. The large proportion of atoms transformed to bcc in Region (a) indicates the preferable growth of bcc phase in low-energy areas, which is the same as for System NW and System KS.

It is worthwhile to note that the transformation at the interfaces with Nagano OR is much slower than at interfaces with NW OR and KS OR in the initial 0.5 ps, which can be seen from the smaller fraction of atoms transformed at each time point in figure 6(d). It is roughly calculated that 53% of atoms on the fcc plane at the original bcc/fcc interfaces transformed to bcc during the first 0.5 ps for System NW, 28% for System KS, followed by 13% for System Nagano. The higher transformation rate for System NW and KS than for System Nagano

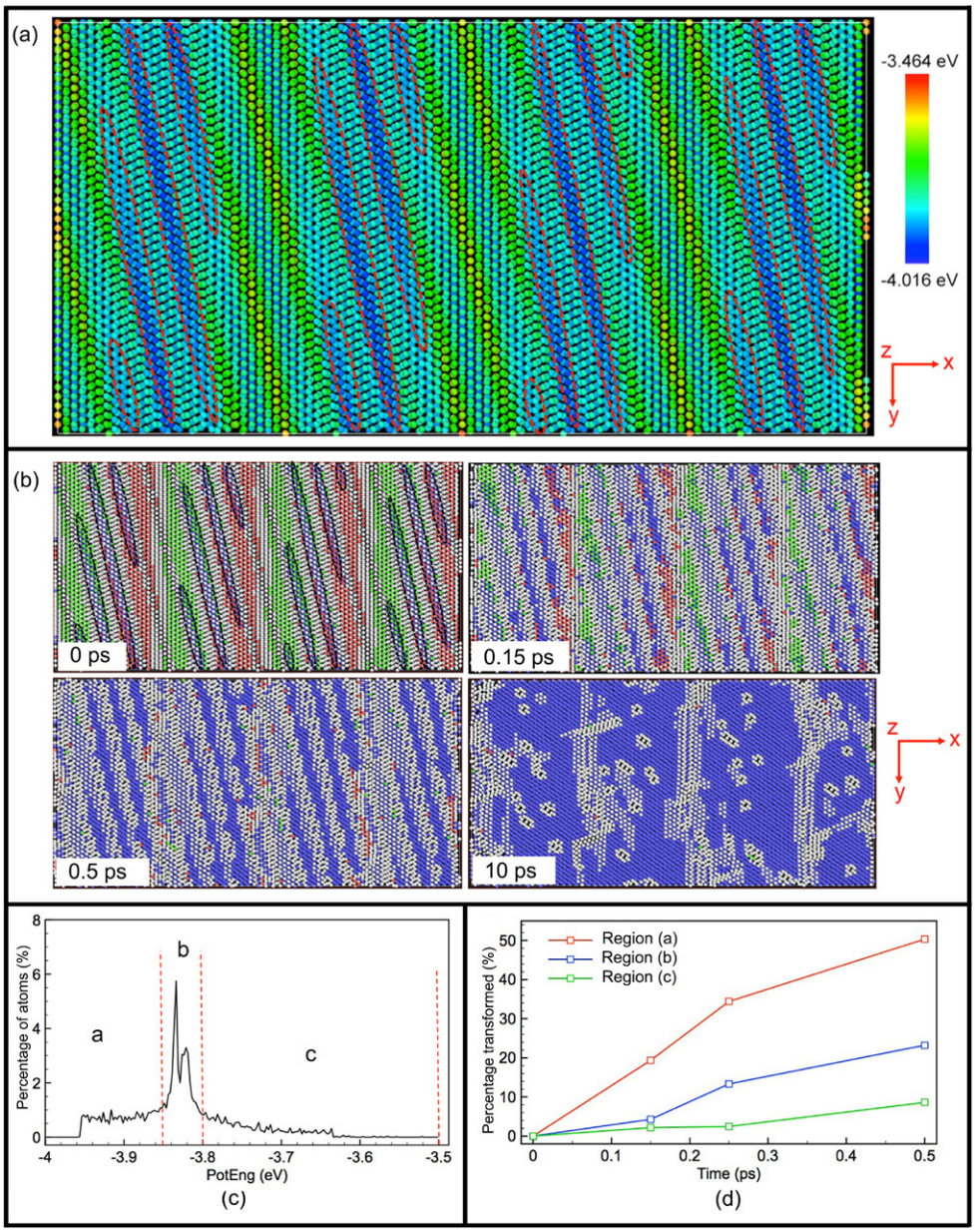

Figure 5. (a) Superposed view of $(1\,1\,1)_{fcc}$ and $(1\,1\,0)_{bcc}$ planes at the matching area of the interface with KS OR at 0 ps. Atoms have been coloured according to their potential energy, as the colour bar shows; (b) Phase transformation in the original fcc/bcc interfacial planes consisting of one fcc layer and one bcc layer in System KS at different simulation times. The colours denote the local crystal structure as in figure 1; (c) Energy distribution of atoms in the fcc monolayer at the original fcc/bcc interface in System KS at 0 ps; (d) Time evolution of the fraction of atoms transformed to bcc in individual regions in the fcc monolayer at the original fcc/bcc interface in the KS OR.

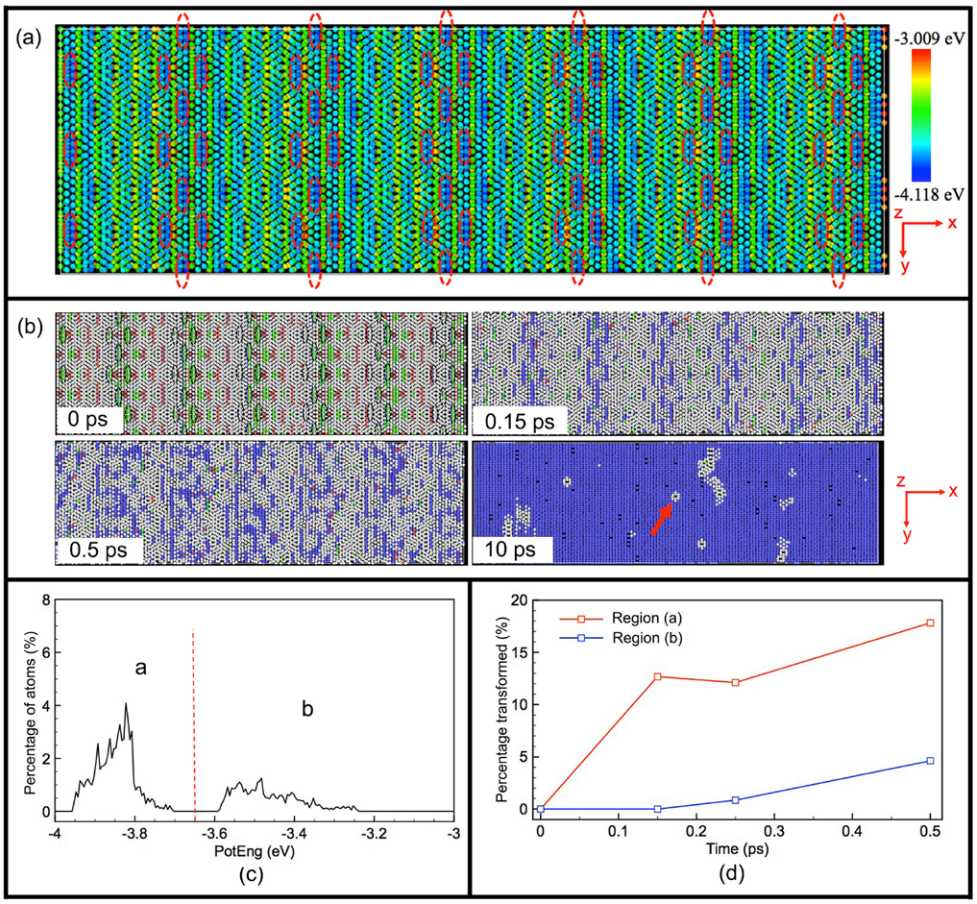

Figure 6. Superposed view of $(1\,1\,\bar{2})_{fcc}$ and $(1\,1\,0)_{bcc}$ planes at the matching area of the interface in the Nagano OR at 0 ps. Atoms have been coloured according to their potential energy, as the colour bar shows; (b) Phase transformation in the original fcc/bcc interfacial planes consisting of one fcc layer and one bcc layer at the interface with Nagano OR at different simulation times. The colours denote the local crystal structure as in figure 1; (c) Energy distribution of atoms in the fcc monolayer at the original fcc/bcc interface in the Nagano OR at 0 ps; (d) Time evolution of the fraction of atoms transformed to bcc in individual regions in the fcc monolayer at the original fcc/bcc interface in the Nagano OR.

indicates that the bcc phase more readily grows at the original bcc/fcc interfaces with NW and KS OR in comparison to the artificial Nagano OR. This may be related to the higher fraction of low-energy interface areas for System NW and System KS than System Nagano, as indicated above. The interface energy contains chemical and mechanical contributions, the latter of which originates from the elastic energy stored in the vicinity of the interface between the austenitic and martensitic phases [31]. Therefore a more perfect interface implies a lower elastic energy and transformation barrier [32]. The less perfect bcc/fcc interface of System Nagano results in higher internal stress, thus higher elastic energy and higher energy barrier for the martensite transformation during the interface propagation. These findings are also in agreement with the abundant occurrence of the KS and NW orientation relation, which are therefore not only based on the nucleation process, but also on growth.

By combining results for the three systems with different bcc/fcc interfaces, it is concluded that growth of original bcc phase in the three semi-coherent bcc/fcc interfaces starts from the areas of low potential energy and develops into high potential energy areas, leaving vacancies in the bcc lattice at the end of the phase transformation. The mechanisms related to this phenomenon will be discussed in detail in the following section.

3.2. Model of growth of original bcc phase at the bcc/fcc interfaces

The growth of original bcc phase starts from low-energy areas and finalizes at high-energy areas at the bcc/fcc interfaces in the three systems. The configurations of fcc and bcc lattices in the low potential energy areas at the original bcc/fcc interfaces in all systems are analyzed in this section.

Figure 7(a) shows the initial growth of original bcc phase in the low-energy areas at the bcc/fcc interface for System NW during 0.15 ps. The areas in which the phase transformation starts are indicated by the yellow dashed triangles and the early transformed atoms are labeled with yellow asterisks. During the fcc-to-bcc transformation, atoms labeled by asterisks tend to move in the direction indicated by the light blue arrows. The configuration of atoms in the two layers after phase transformation is labeled by the light blue parallelogram. Similar to figures 7(a)–(c) show the corresponding configurations in low energy locations for System KS and System Nagano, respectively. The early transformed atoms and the atomic configurations of two $\{1\,1\,0\}_{\mathrm{bcc}}$ planes are marked by asterisks and parallelograms, respectively. Also these details of the atomic configurations show that the growth of the original bcc phase starts from the low-energy areas at the original bcc/fcc interfaces for System NW, System KS and System Nagano.

The configuration of atoms in the fcc and bcc planes at the initial configuration in this low-energy area was previously reported by Olson and Cohen [33], as shown in figure 8(a). They developed a faulting mechanism for the complete fcc-to-bcc lattice deformation based on the 'hard sphere' lattice deformation model suggested by Bogers and Burgers [34]. They illustrated the fcc-to-bcc transformation through two shears: the first shear takes place over one-third of the Burgers vector of a Shockley partial dislocation for fcc twin shear ($a_{\mathrm{fcc}}/18\ \langle 1\,1\,2\rangle$ on $\{1\,1\,1\}_{\mathrm{fcc}}$ plane); the second shear corresponds to three-eighths of a Shockley partial dislocation for fcc twin shear ($a_{\mathrm{fcc}}/16\ \langle 1\,1\,2\rangle_{\mathrm{fcc}}$ on the $\{1\,1\,1\}_{\mathrm{fcc}}$ plane or $1/8\ a_{\mathrm{bcc}}\ \langle 1\,1\,0\rangle_{\mathrm{bcc}}$ on the $\{1\,1\,0\}_{\mathrm{bcc}}$ plane). After the first shearing in the $\{1\,1\,1\}_{\mathrm{fcc}}$ plane, each atom advances to a saddle-point position, which was energetically achievable under the given thermal and thermodynamic conditions. Figure 8(a) shows the configuration of planes obtained at the saddle-point position. In order to obtain the actual configuration of $\{1\,1\,0\}_{\mathrm{bcc}}$ planes, which is shown by the blue parallelogram, a second shear is taking place, with a displacement of $a_{\mathrm{fcc}}/16\ \langle 1\,1\,2\rangle_{\mathrm{fcc}}$, as shown by the blue arrow in figure 8(a).

A similar configuration of atoms to figure 8(a), which are chosen inside the yellow triangles in figure 7(a), is observed at the original bcc/fcc interfaces for System NW, especially those marked by asterisks and the successive layer of atoms. The corresponding snapshots before and after phase transformation are shown in figure 8(b). Compared with the model by Bogers and Burgers [34], these atoms are already at the positions of the saddle-point and thus no first shear is involved. The transformation to the bcc structure involved a displacement of $a_{\mathrm{fcc}}/16\ \langle 1\,1\,2\rangle$ referred to the fcc structure [34]. This corresponds to a shearing displacement of $a_{\mathrm{fcc}}/16\ [1\,1\,\bar{2}]_{\mathrm{fcc}}$ in the negative x direction, as the light blue arrow shows. Similarly, the successive fcc-to-bcc transformation for the atoms identified with an fcc structure in snapshot at 0 ps in figure 7(a) involves a shearing displacement of $a_{\mathrm{fcc}}/16\ [\bar{1}\bar{1}2]_{\mathrm{fcc}} \parallel [\bar{1}\ 1\ 0]_{\mathrm{bcc}}$ in the positive x direction.

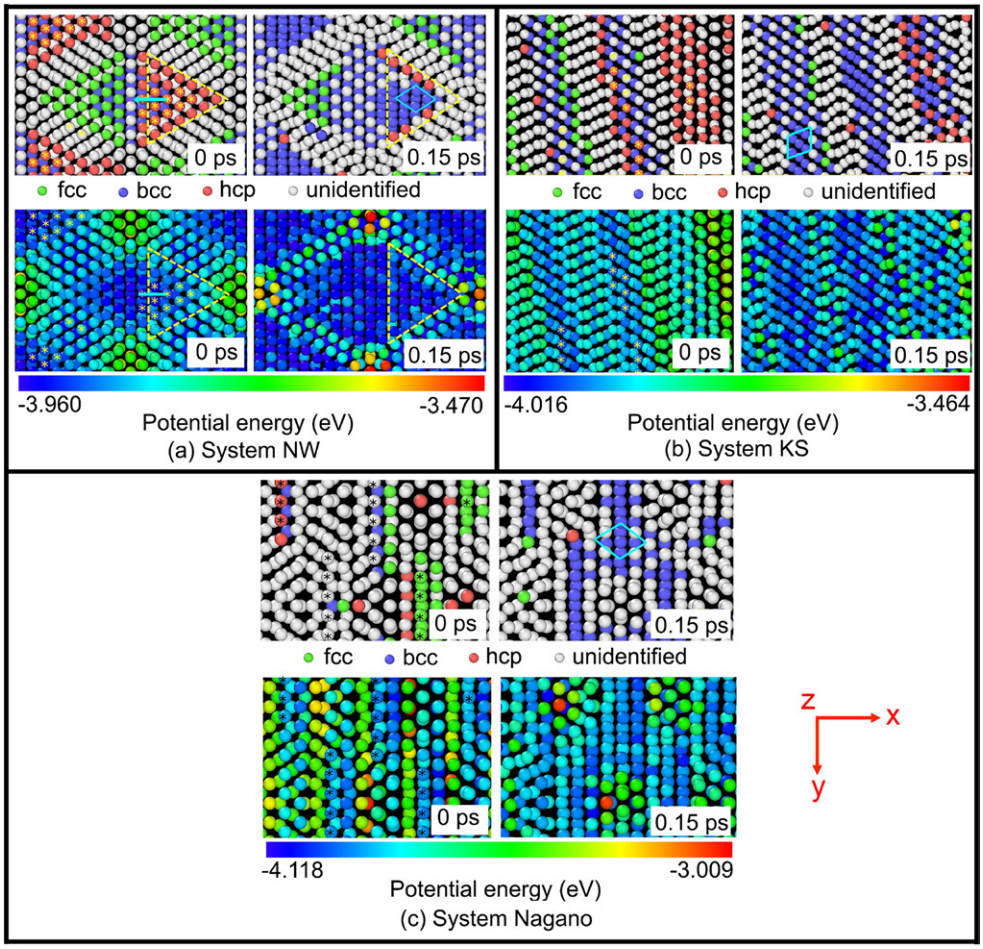

Figure 7. (a) Enlarged superposed view of $(1\,1\,1)_{fcc}$ and $(1\,1\,0)_{bcc}$ planes at the interface with NW OR at different simulation times; (b) Enlarged superposed view of $(1\,1\,1)_{fcc}$ and $(1\,1\,0)_{bcc}$ planes at the interface with KS OR at different simulation times; (c) Enlarged superposed view of $(1\,1\,\bar{2})_{fcc}$ and $(1\,1\,0)_{bcc}$ planes at the interface in System Nagano at different simulation times.

The configuration of atoms in the low potential energy area at the original bcc/fcc interface before and after the fcc-to-bcc phase transformation is shown in figure 8(c) for System KS and in figure 8(d) for System Nagano, respectively. The light blue parallelograms indicate the regular configuration of $(1\,1\,0)_{bcc}$ planes and the light blue arrows illustrate the displacement in the direction $[\bar{1}\ 1\ 0]_{bcc}$. It is found that System KS and System Nagano share the same shearing model [33, 34] with System NW regarding the growth of original bcc phase at the bcc/fcc interfaces in low potential energy locations.

From the above, the growth of original bcc phase in low potential energy areas in the three systems share the same faulting mechanism proposed by Olson and Cohen [33] based on Bogers and Burgers' initial concept [31]. Yang *et al* [24, 25] verified the 'two-shear' Bogers–Burgers–Olson–Cohen (BBOC) model experimentally after examining the deformation-induced martensitic transformation in an austenitic stainless steel with high-resolution transmission electron microscopy (HRTEM). The two shears of 'T/3-3/8T' (T represents a Shockley partial

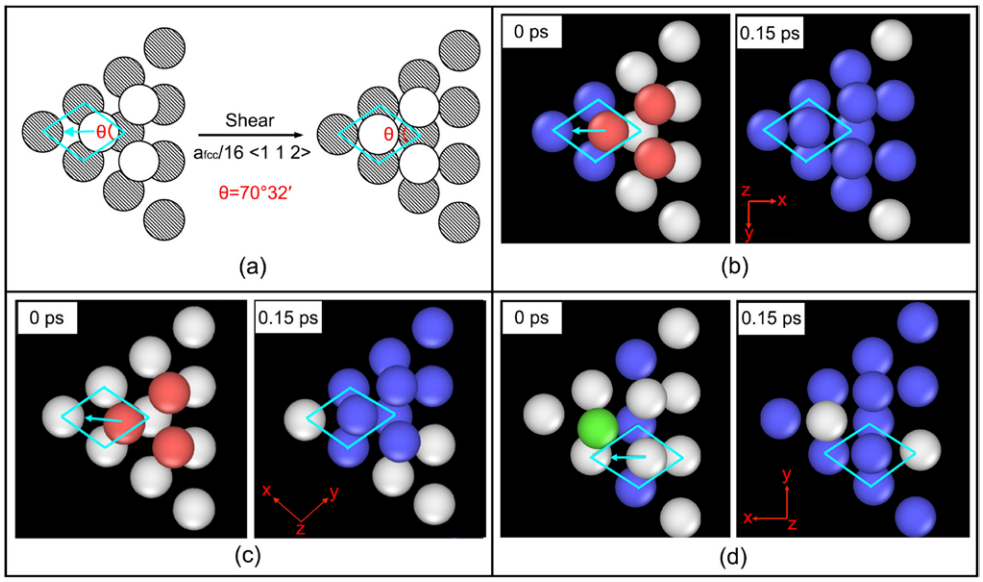

Figure 8. (a) Configuration of $\{1\,1\,0\}_{\mathrm{bcc}}$ type planes after the $a_{\mathrm{fcc}}/18\,\langle 1\,1\,2\rangle$ in the $\{1\,1\,1\}_{\mathrm{fcc}}$ plane and the proper configuration in a regular bcc structure after the successive shearing of these $\{1\,1\,0\}_{\mathrm{bcc}}$ type planes. The mechanism was previously reported in [33, 34]; (b)–(d) Corresponded configurations of atoms at the interface for System NW (b), System KS (c) and System Nagano (d) at 0 ps and 0.15 ps. The colours of atoms in (b)–(d) denote the local crystal structure as in figure 1.

dislocation for fcc twin shear) during the deformation-induced γ(fcc) $\rightarrow$ ε(hcp) $\rightarrow$ α'(bcc) phase transformation was confirmed with the HRTEM observations, as well as with their MD simulation results of the interfaces between the γ and α' with Pitsch OR and two KS orientation relations. In the present simulations, however, the detailed study into the atomic displacements during the phase transformation at the bcc/fcc interfaces indicates that the model does not apply entirely, but only locally, i.e. in the low potential energy areas at the bcc/fcc interfaces. Furthermore, only the second shear but not the first one is involved during the growth of original bcc phase. The absence of the first shear may explain the relatively rapid fcc-to-bcc transformation at the low-energy areas at the bcc/fcc interfaces. For the high-energy areas at the interfaces, however, diffusion might be needed for atoms to reach their equilibrium positions so as to obtain the true bcc lattices.

3.3. Displacement of the atoms involved in the growth of the bcc phase at the bcc/fcc interface

Figure 9(a) shows the local snapshot of one mono bcc plane with atoms marked by 3D vectors showing their displacements in the first 10 ps. The plane corresponds to the fcc-plane at the original bcc/fcc interface with NW OR. Atoms with low potential energies inside the red triangle are found to move in a collective movement for a small displacement and the neighbouring atoms of each atom remain unchanged. For atoms with higher initial potential energies, the displacements tend to be larger. A small portion of atoms with high potential energies involves a displacement on the order of an interatomic distance or larger. Those atoms at the high-energy areas move randomly, with characteristics of diffusional jumps of atoms. Vacancies appear where the diffusional jump is observed, as is labeled by the small red

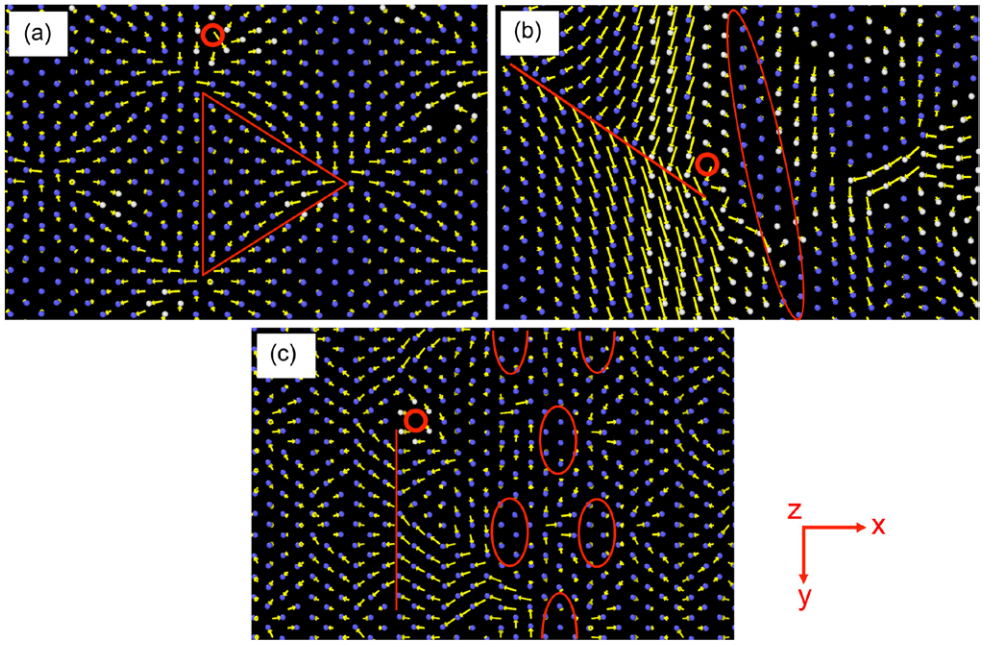

Figure 9. Snapshots of atoms with 3D displacement vectors for System NW (a), System KS (b) and System Nagano (c). The local regions involved in (a)–(c) belong to the mono fcc-plane at the interfaces and the corresponding displacements are calculated at 10 ps.

circle. The high-energy areas also display the change of neighboring atoms and the creation of new atomic arrangement.

Similar to that of System NW, the growth of bcc phase at the low energy areas at the interfaces also involves a locally collective motion of atoms with small displacements for System KS and System Nagano, as shown by the red ellipses in figures 9(b) and (c), respectively. By comparing the displacement vectors of atoms on both sides of the red lines at high energy areas in figures 9(b) and (c), the collective motion of atoms on one side of the red lines is neighboured on the other side by another group of atoms moving collectively in a different direction. Despite the collective motion, the atomic displacements for either group of atoms are on the order of or even higher than one interatomic distance. For the two layers of atoms alongside the red lines, they lose their original neighbours due to their large displacements in different directions. Thus the atomic neighbours change and defects such as vacancies, as labeled by the small red circles, are found in these areas.

Figure 10(a) indicates the corresponding displacement distribution of atoms in figure 9(a) for System NW. It is found that 99.9% of atoms undergo a displacement less than 2.4 Å for System NW. Combined with the above results, the growth of original bcc phase at the original bcc/fcc interfaces with the NW OR involves a mixed mechanism, which is of a predominantly martensitic nature in the low potential energy areas and a possibly diffusional nature for some of the atoms in high potential energy areas. For System KS, 90.3% of the atoms undergo a displacement smaller than 2.4 Å, as shown in figure 10(b). Similar to System NW, the growth of bcc phase in low potential energy areas is of a martensitic nature. The growth of bcc phase in the high energy areas in System KS may involve in a diffusional mechanism. The result in figure 10(c) indicates that approximately 99.2% of atoms have a displacement less than 2.4 Å for System Nagano. The final 0.8% atoms belong to the ones located at high potential energy positions and may involve diffusional displacement.

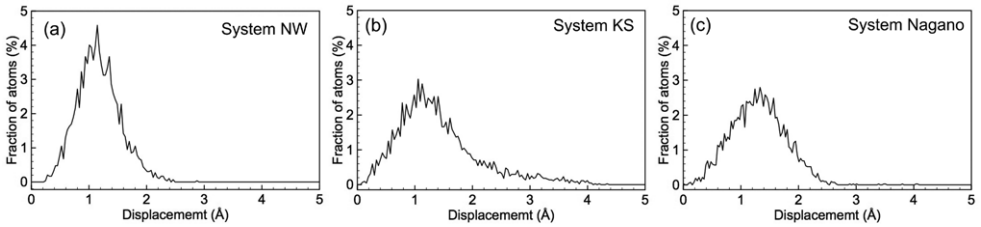

Figure 10. Displacement distribution of atoms on the mono fcc-plane at the interfaces for System NW (a), System KS (b) and System Nagano (c) at 10 ps.

From the present analysis, a predominantly martensitic mechanism is confirmed for the growth of original bcc phase in the low potential energy areas at the bcc/fcc interfaces for System NW, System KS and System Nagano. However, diffusional jumps of atoms may be involved during the growth of bcc phase in the high potential energy areas. A higher fraction of atoms with a displacement on the order of one interatomic distance is found in System KS than in System NW and System Nagano. This indicates that more atoms are involved in the diffusional transformation during the growth of bcc/fcc interfaces in System KS. This is shown to be leading to more defects, i.e. vacancies, in the high-energy areas at the final configuration. The defects may pin the further propagation of the bcc/fcc interfaces, but also act as the preferred nucleation sites for new bcc phase inside the original fcc phase. Besides, the displacements of atoms in the low potential energy areas are much smaller than those in the high potential energy areas. The absence of the first shear during the fcc-to-bcc transformation as first proposed by Bogers and Burgers [34] and later by Olson and Cohen [33], may explain the smaller displacements for atoms at the low potential energy areas at the bcc/fcc interfaces.

4. Conclusions

MD simulations were performed using the Mendelev potential [23] to study the mechanisms controlling the growth of the original bcc phase during the fcc-to-bcc transformation in three systems with semi-coherent bcc/fcc interfaces, which are NW, KS and Nagano orientation relationships, respectively. Simulations show that:

- The bcc/fcc interfaces of System NW, System KS and System Nagano propagate into the fcc bulk involving a limited number of atomic layers in a facetted style. The propagation of the bcc/fcc interface following a facetted style is also observed in the MD simulation of the bcc/fcc interface in the NW OR in iron using the Ackland potential [22]. The same transformation mechanism at the interfaces has been observed with the two different potentials.
- Growth of bcc phase starts in the areas of low potential energy at the original bcc/fcc interfaces and develops into the high-energy areas.
- Growth of bcc phase at low potential energy areas follows the faulting mechanism proposed by Olson and Cohen [33] based on the Bogers–Burgers model [34]. A collective motion of atoms is involved and is of a martensitic character.
- The MD simulations indicate that growth of bcc phase in the high potential energy areas at the original fcc/bcc interfaces involves diffusional atomic jumps for a small fraction of the atoms.

Acknowledgments

The research leading to these results has received funding from the European Research Council under the European Union's Seventh Framework Programme FP7/2007–2013/ERC grant agreement no [306292]. The authors would like to thank Prof Barend J Thijsse and Dr Peter Klaver from Delft University of Technology, the Netherlands, and Prof Chad Sinclair from the University of British Columbia, Canada, for the fruitful discussions.

References

[1] Roitburd A L and Kurdjumov G V 1979 The nature of martensitic transformations *Mater. Sci. Eng.* **39** 141–67
[2] Santofimia M J, Zhao L, Petrov R, Kwakernaak C, Sloof W G and Sietsma J 2011 Microstructural development during the quenching and partitioning process in a newly designed low-carbon steel *Acta Mater.* **59** 6059–68
[3] Bunshah R F and Mehl R F 1953 The rate of propagation of martensite *Trans. AIME* **197** 1251–8
[4] Bos C, Sietsma J and Thijsse B J 2006 Molecular dynamics simulation of interface dynamics during the fcc–bcc transformation of a martensitic nature *Phys. Rev.* B **73** 104117
[5] Wang B J, Sak-Saracino E, Gunkelmann N and Urbassek H M 2014 Molecular-dynamics study of the α–γ phase transition in Fe–C *Comput. Mater. Sci.* **82** 399–404
[6] Yang Z and Johnson R A 1993 An EAM simulation of the alpha–gamma iron interface model *Simul. Mater. Sci. Eng.* **1** 707–16
[7] Nagano T and Enomoto M 2006 Calculation of the interfacial energies between α and γ iron and equilibrium particle shape *Metall Mater. Trans.* A **37** 929–37
[8] Bain E C and Dunkiri N Y 1924 The nature of martensite *Trans. Am. Inst. Min. Metal. Eng.* **70** 25–47
[9] Miyamoto G, Takayama N and Furuhara T 2009 Accurate measurement of the orientation relationship of lath martensite and bainite by electron backscatter diffraction analysis *Scr. Mater.* **60** 1113–6
[10] Nishiyama Z 1934 X-ray investigation of the mechanism of the transformation from face-centred to body-centred cubic lattice *Sci. Rep. Tohoku Imp. Univ.* **23** 637–64
[11] Kurdjumov G V and Sachs G 1930 About the Mechanism of Steel Hardening *Z. Phys.* **64** 325–43
[12] Tateyama S, Shibuta Y and Suzuki T 2010 Orientation relationship in fcc–bcc phase transformation kinetics of iron: a molecular dynamics study *ISIJ Int.* **50** 1211–6
[13] Tateyama S, Shibuta Y and Suzuki T 2008 A molecular dynamics study of the fcc–bcc phase transformation kinetics of iron *Scr. Mater.* **59** 971–4
[14] Wang B J and Urbassek H M 2014 Atomistic dynamics of the bcc–fcc phase transition in iron: competition of homo- and heterogeneous phase growth *Comput. Mater. Sci.* **81** 170–7
[15] Wang B J and Urbassek H M 2013 Molecular dynamics study of the α–γ phase transition in Fe induced by shear deformation *Acta Mater.* **61** 5979–87
[16] Song H and Hoyt J J 2013 An atomistic simulation study of the migration of an austenite–ferrite interface in pure Fe *Acta Mater.* **61** 1189–96
[17] Song H and Hoyt J J 2012 A molecular dynamics simulation study of the velocities, mobility and activation energy of an austenite–ferrite interface in pure Fe *Acta Mater.* **60** 4328–35
[18] Wang B J and Urbassek H M 2013 Phase transitions in an Fe system containing a bcc/fcc phase boundary: An atomistic study *Phys. Rev.* B **87** 104108
[19] Tateyama S, Shibuta Y, Kumagai T and Suzuki T 2011 A molecular dynamics study of bidirectional phase transformation between bcc and fcc iron *ISIJ Int.* **51** 1710–6
[20] Johnson R A and Oh D J 1989 Analytic embedded atom method model for bcc metals *J. Mater. Res.* **4** 1195–201
[21] Meyer R and Entel P 1998 Martensite-austenite transition and phonon dispersion curves of $Fe_{1-x}Ni_x$ studied by molecular-dynamics simulations *Phys. Rev.* B **57** 5140–7
[22] Ackland G J, Bacon D J, Calder A F and Harry T 1997 Computer simulation of point defect properties in dilute Fe–Cu alloy using a many-body interatomic potential *Phil. Mag.* A **75** 713–32

[23] Mendelev M I, Han S, Srolovitz D J, Ackland G J, Sun D Y and Asta M 2003 Development of new interatomic potentials appropriate for crystalline and liquid iron *Phil. Mag.* **83** 3977–94
[24] Yang X S, Sun S, Wu X L, Ma E and Zhang T Y 2014 Dissecting the mechanism of martensitic transformation via atomic scale observations *Sci. Rep.* **4** 6141
[25] Yang X S, Sun S and Zhang T Y 2015 The mechanism of bcc α' nucleation in single hcp ε laths in the fcc $\gamma \rightarrow$ hcp $\varepsilon \rightarrow$ bcc α'; martensitic phase transformation *Acta Met.* **95** 264–73
[26] Müller M, Erhart P and Albe K 2007 Analytic bond-order potential for bcc and fcc iron-comparison with established embedded-atom method potentials *J. Phys.: Condens. Matter* **19** 326220
[27] Van der Merwe J H and Shiflet G J 1994 The role of structural ledges at phase boundaries; 1: Interfaces with rectangular atomic nets *Acta Mater.* **42** 1199–205
[28] http://lammps.sandia.gov/
[29] Stukowski A 2012 Structure identification methods for atomistic simulations of crystalline materials *Modell. Simul. Mater. Sci. Eng.* **20** 045021
[30] Stukowski A 2010 Visualization and analysis of atomistic simulation data with OVITO-the open visualization tool *Modelling Simul. Mater. Sci. Eng.* **18** 015012
[31] Waitz T, Antretter T, Fischer F D, Simha N K and Karnthaler H P 2007 Size effects on the martensitic phase transformation of NiTi nanograins *J. Mech. Phys. Solids* **55** 419–44
[32] Lei C H, Li L J, Shu Y C and Li J Y 2010 Austenite–martensite interface in shape memory alloys *Appl. Phys. Lett.* **96** 141910
[33] Olson G B and Cohen M 1976 A general mechanism of martensitic nucleation- part II. FCC $\rightarrow$ BCC and other martensitic transformations *Metall. Trans.* A **7** 1905–14
[34] Bogers A J and Burgers W G 1964 Partial dislocations on the $\{1\,1\,0\}$ planes in the bcc lattice and the transition of the fcc into the bcc lattice *Acta Met.* **12** 255–61